Cerebral Cortex March 2009;19:511-523
doi:10.1093/cercor/bhn101
Advance Access publication June 11, 2008

Synapsin- and Actin-Dependent Frequency Enhancement in Mouse Hippocampal Mossy Fiber Synapses

Simen G. Owe[1,2], Vidar Jensen[3], Emma Evergren[4], Arnaud Ruiz[5], Oleg Shupliakov[4], Dimitri M. Kullmann[5], Jon Storm-Mathisen[1,2], S. Ivar Walaas[3], Øivind Hvalby[3] and Linda H. Bergersen[1,2]

[1]Department of Anatomy, Institute of Basic Medical Sciences, [2]Centre for Molecular Biology and Neuroscience, [3]Molecular Neurobiology Research Group, Institute of Basic Medical Sciences, University of Oslo, PO Box 1105, Blindern, N-0317 Oslo, Norway, [4]Department of Neuroscience, Linné Centre for Developmental Biology and Regenerative Medicine, Karolinska Institutet, 17177 Stockholm, Sweden and [5]Institute of Neurology, University College London, London WC1N 3BG, UK

Simen G. Owe and Vidar Jensen contributed equally to this work

The synapsin proteins have different roles in excitatory and inhibitory synaptic terminals. We demonstrate a differential role between types of excitatory terminals. Structural and functional aspects of the hippocampal mossy fiber (MF) synapses were studied in wild-type (WT) mice and in synapsin double-knockout mice (DKO). A severe reduction in the number of synaptic vesicles situated more than 100 nm away from the presynaptic membrane active zone was found in the synapsin DKO animals. The ultrastructural level gave concomitant reduction in F-actin immunoreactivity observed at the periactive endocytic zone of the MF terminals. Frequency facilitation was normal in synapsin DKO mice at low firing rates (~0.1 Hz) but was impaired at firing rates within the physiological range (~2 Hz). Synapses made by associational/commissural fibers showed comparatively small frequency facilitation at the same frequencies. Synapsin-dependent facilitation in MF synapses of WT mice was attenuated by blocking F-actin polymerization with cytochalasin B in hippocampal slices. Synapsin III, selectively seen in MF synapses, is enriched specifically in the area adjacent to the synaptic cleft. This may underlie the ability of synapsin III to promote synaptic depression, contributing to the reduced frequency facilitation observed in the absence of synapsins I and II.

Keywords: actin filaments, frequency facilitation, hippocampal synapses, immunoelectron microscopy, presynaptic plasticity

Short-term activity-induced synaptic plasticity depends in large part on highly dynamic synaptic vesicle trafficking (Greengard et al. 1993; Hilfiker et al. 1999; Zucker and Regehr, 2002). It is believed that the synapsin family of phosphoproteins, encoded by 3 distinct genes each of which gives rises to several splice variants, is involved in the organization of vesicles in a majority of central synapses (see reviews Kao et al. 1998; Hilfiker et al. 1999; Evergren et al. 2007). Early in situ studies (Greengard et al. 1993; Pieribone et al. 1995; Rosahl et al. 1995; Takei et al. 1995), later supported by experiments on neuronal cell cultures (Terada et al. 1999; Gitler et al. 2004), indicated that the synapsins are predominantly involved in regulating the packing density of synaptic vesicles by linking them to actin filaments and controlling the size of the cytoplasmic presynaptic vesicle cluster, mainly representing a "reserve pool" (RP) of vesicles, without affecting the "readily releasable pool" (RRP) of vesicles, docked to the presynaptic membranes (Ryan et al. 1996; Hilfiker et al. 1999; Feng et al. 2002). Synapsin proteins are actin-nucleating agents and promote F-actin polymerization, thereby regulating cytoskeletal–vesicle interactions (Bahler and Greengard 1987; Benfenati et al. 1989; Hilfiker et al. 1999; Shupliakov et al. 2002; Bloom et al. 2003). Other studies, however, have proposed additional functions, for example, involvement of synapsins in the regulation of vesicle fusion (Hilfiker et al. 1998) and synaptic vesicle recycling (Bloom et al. 2003), and the relative importance of these phenomena may vary in different populations of synapses, for example, excitatory versus inhibitory synapses (Gitler et al. 2004; Bogen et al. 2006; Hvalby et al. 2006; Kielland et al. 2006). Some central synapses have also been reported to lack synapsins (Kielland et al. 2006). To further address the question of the functional role of synapsins in central nervous system (CNS), we have examined glutamatergic signaling in 2 types of synapses with different morphological and short-term plasticity properties: terminals of hippocampal mossy fibers (MFs) and terminals formed by the recurrent associational/commissural (AC) collaterals, that is, the 2 principal synaptic pathways in hippocampus and parts of neuronal circuits controlling memory functions.

The MF originate from the granule cells in the dentate area and innervate the proximal pyramidal cell dendritic spines located in the stratum lucidum of the CA3 region (Blackstad and Kjaerheim 1961) with giant terminals, each containing 30–40 vesicle clusters at active zones (Chicurel and Harris 1992; Rollenhagen et al. 2007), with approximately 1400 RRP vesicles (Hallermann et al. 2003) and a total of approximately 10 000 cytoplasmic RP vesicles per terminal (Bischofberger et al. 2006). These synapses have a unique ability to tune synaptic transmission to a wide range of firing frequencies, the prevailing physiological range being about 0.5–4 Hz (Bischofberger et al. 2006), whereby responses can undergo a pronounced frequency facilitation (Salin et al. 1996).

In contrast, very small terminals are formed by the AC collaterals, which derive from the CA3 pyramidal cells and terminate in both ipsilateral and contralateral CA1–CA3 regions to form axospinous excitatory synapses on pyramidal cell dendrites, the ipsilateral collaterals to stratum radiatum of CA1 being known as Schaffer collaterals (Blackstad 1956; Hjorth-Simonsen 1973; Witter et al. 2000). These small boutons, usually with one active zone, have 5–10 RRP vesicles, about 80 vesicles in the recycling pool and a total of 100–200 vesicles (Harris and Sultan 1995; Schikorski and Stevens 1997; Ryan et al. 2001). AC collateral synapses generally exhibit less marked frequency facilitation than MF giant synapses and tend to depress in response to prolonged trains of intermediate frequency stimulation (Salin et al. 1996; Nicoll and Schmitz 2005; Hvalby et al. 2006).

The functional importance of the synapsin proteins in these synapses remains unclear. Genetic ablation of synapsin I (Takei et al. 1995) or synapsins I + II (Spillane et al. 1995) changed

neither baseline field excitatory postsynaptic potentials (fEPSPs) nor long-term potentiation at MF–CA3 pyramidal cell synapses. In contrast, genetic deletion of synapsins I + II led to strong response depression in the AC synapses in the CA1 stratum radiatum (e.g., Rosahl et al. 1995; Hvalby et al. 2006; Jensen et al. 2007). The number of releasable vesicles in different terminals may be a limiting factor behind some of these effects, but other mechanisms may also contribute (e.g., Dobrunz and Stevens 1997; Stevens and Wesseling 1998; Delgado et al. 2000; Millar et al. 2002; Zucker and Regehr 2002; Bloom et al. 2003; Evergren et al. 2007; Jensen et al. 2007; Lisman et al. 2007). In the present study, we focused on possible involvement of actin and synapsin in glutamate release in MF and AC terminals. Experiments were performed in wild-type (WT) and synapsin I + II double-knockout (DKO) mice. Perturbation of actin filament formation was induced by the F-actin severing agent, cytochalasin B. Our results indicate that the strong and prolonged frequency facilitation induced by the MF terminals at physiological stimulation frequencies consists of 2 parts, one of which is strongly synapsin and F-actin dependent. In contrast, the AC synapses showed small and almost synapsin- and actin-independent frequency facilitation. Parts of this study have been presented in abstract form (Gylterud et al. 2004; Gylterud Owe et al. 2007).

Materials and Methods

Animals

Animal experiments were approved by, and performed in accordance with, guidelines of the Norwegian Animal Welfare Act and the European Union's Directive 86/609/EEC.

Synapsin DKO mice, as described in Ferreira et al. (1998), and WT mice were used for comparative ultrastructural and electrophysiological studies. Animals were given free access to food and water. Experiments and analyses were performed blinded with regard to the genotype.

Antibodies

Antibody to F-actin was obtained from Chemicon International (Hampshire, UK) (mouse, monoclonal, C4). The synapsin rabbit polyclonal anti-E domain antibody (G304) recognizing synapsins Ia, IIa, and IIIa was a gift from P. Greengard's laboratory (Rockefeller University, NY). The antibody has been characterized previously (Kao et al. 1998).

Tissue Preparation, Perfusion-Fixed Material

Five synapsin DKO and 5 WT mice, 3–6 months old, were used to quantify the number of vesicles in hippocampal synapses and the labeling density of synapsin. Mice were deeply anesthetized by an intraperitoneal injection of equithesin (0.3 ml per 100 g body weight, Rikshospitalets Apotek, Oslo, Norway) and subjected to transcardiac perfusion with a mixture of glutaraldehyde (GA, 0.1%) and paraformaldehyde (PFA, 4%) in 0.1 M sodium phosphate (NaPi) buffer, pH 7.4.

The tissue was processed as described earlier (Bergersen et al. 2001). Briefly, specimens (typically 0.5 × 0.5 × 1 mm) from hippocampus were cryoprotected by immersion in graded concentrations of glycerol (10%, 20%, and 30%) in 0.1 M NaPi for 30 min at each step and then overnight in 30% glycerol in 0.1 M NaPi overnight at 4 °C. Samples were then plunged into liquid propane cooled at –190 °C by liquid nitrogen in a Universal Cryofixation System KF80 (Reichert-Jung, Vienna, Austria). Tissue blocks were moved by a precooled forceps. For freeze substitution, tissue samples were immersed in a solution of 0.5% uranyl acetate in anhydrous methanol and kept overnight at –90 °C. The temperature was raised stepwise in 4 °C increments per hour from –90 to –45 °C, where it was kept for the subsequent steps. Thereafter, tissue samples were washed several times with anhydrous methanol to remove residual water and uranyl acetate. The infiltration in Lowicryl HM20 (Polysciences, Washington, PA) went stepwise from Lowicryl:methanol 1:2, 1:1, and 2:1 (1 h each) to pure Lowicryl (overnight). For polymerization, the tissue was placed in a precooled embedding mall and exposed to ultraviolet light at a wavelength of 360 nm for 2 days at –45 °C followed by 1 day at room temperature. Ultrathin sections (80 nm) were cut with a diamond knife on a Reichert-Jung ultramicrotome and mounted on nickel grids using an adhesive pen (David Sangyo, Japan).

Slice Preparations

In order to determine the ultrastructure of the MF and AC synapses following experimental manipulations, slice preparations were analyzed following exposure to high [KCl] (Wickelgren et al. 1985) and in the absence or presence of cytochalasin B. Adult WT or synapsin DKO animals were sacrificed with the general anesthetic desflurane (Suprane, Baxter), the brains were removed, and transverse slices (400 μm) were cut from the middle portion of each hippocampus with a vibroslicer in artificial cerebrospinal fluid (ACSF, 4 °C, bubbled with 95% O_2–5% CO_2, pH 7.4) containing (in mM): 124 NaCl, 2 KCl, 1.25 KH_2PO_4, 2 $MgSO_4$, 1 $CaCl_2$, 26 $NaHCO_3$, and 12 glucose. Slices were placed in a humidified interface chamber at 28–32 °C and perfused with ACSF containing 2 mM $CaCl_2$.

Slices from both genotypes were divided into 4 groups (3 mice per group), with groups 1 and 2 kept in normal ACSF, whereas groups 3 and 4 were kept in ACSF containing cytochalasin B (20 μM). Synaptic efficacy in the slices during incubations was characterized by continuous monitoring of fEPSPs (0.1-Hz test stimulation) in the CA3-to-CA1 stratum radiatum AC synapse as described (Hvalby et al. 2006). Following equilibration with or without cytochalasin B, slices from groups 2 and 4 were subjected to 30 mM KCl added to the perfusing medium.

When correlative analyses of these slices were performed after electrophysiological stimuli and recordings, they were treated as above, only they were fixed in 4% PFA and 2.5% GA, rinsed in NaPi, then treated with 1% OsO_4 in 0.1 M NaPi, dehydrated in graded ethanol followed by propylene oxide, and embedded in Durcupan (Fluka, Buchs, Switzerland).

Quantitative Electron Microscopic Vesicle Analyses

Ultrathin sections covering the CA1 region and the dentate gyrus including the hilus or covering the CA3 region were contrasted with uranyl acetate (5% in 40% ethanol) and lead citrate (0.3%), and digital pictures of AC terminals in CA1 (Schaffer collaterals) and MF terminals either in the hilus (perfusion-fixed material) or in the stratum lucidum of CA3 (acute slices) were taken at a primary magnification of 11 000–26 500× (at least 20 pictures per area per animal), in a Philips CM 100 or a Tecnai 12 FEI electron microscope, both equipped with digital cameras. The MF terminals were identified based on size, presence of clearly defined asymmetrical synapses, and the specific protrusion of dendritic spines into the larger terminals. The AC terminals were identified by having asymmetrical synapses and by location onto dendritic spines situated close to apical dendrites in the stratum radiatum region.

For analyses of vesicle density, the distance from each vesicle to the presynaptic membrane, opposed to a postsynaptic density, was determined. This was done by recording the Cartesian coordinates of the vesicle centers that were then used to automatically calculate vesicle densities within given distances from the synapse. Calculations were performed as follows: a second-degree polynomial equation for the presynaptic membrane was constructed, representing a parabola, using 3 known coordinates that were along the synaptic cleft and in the active zone. To find the minimum distance between a point marked at the center of each vesicle and the parabola representing the presynaptic membrane, a second function describing this distance was constructed (eq. 1):

$$D = \sqrt{(x-p)^2 + (f(x)-q)^2},$$

where x and $f(x)$ are the coordinates for a point along the parabola, and p and q are the vesicle coordinates. The minimum distance was

found where the derivative of equation (1) was equal to zero, using a Maple (Waterloo Maple, Ontario, Canada) plug-in for Excel (Microsoft, Redmond, WA). A line between the ends of the postsynaptic density was used to construct a perpendicular lateral limit (Fig. 1*A*). The area was determined by the distance between the 2 lateral limits and by grouping the distances into bins of 50 nm. Areas occupied by organelles other than synaptic vesicles (mitochondria, endoplasmic reticulum, and plasma membrane) or outside the terminal were excluded. Also, the vesicles were grouped into the distances 0–100 nm and 100–400/500 nm as stated in the figure legends. Albeit not the same as the functionally defined vesicle pools RRP and RP, this grouping is thought to reflect these areas. If more than one synapse was within the same terminal, they were analyzed by first defining both the RRPs and then splitting the RP between the 2 if they overlapped.

Quantitative Electron Microscopic Postembedding Immunogold Labeling

Immunocytochemistry was performed on ultrathin sections to specifically localize and quantify F-actin and synapsins in terminals. F-actin labeling was compared between WT and synapsin DKO mice, whereas synapsin labeling was performed to compare MF terminals with AC terminals in WT mice and find the subcellular localization of synapsin III, by using the panspecific antibody G304 in synapsin I + II DKO mice (Pieribone et al. 2002).

For synapsin analyses, perfusion-fixed hippocampi were used, embedded as described above. In the case of F-actin analyses, slices were prepared and treated as described in the Electrophysiological Analysis (but without DL-2-amino-5-phosphonopentanoic acid [AP5]) and eventually exposed to 40 mM [KCl]. These slices were removed 4 min after the disappearance of the electric response, fixed in cold

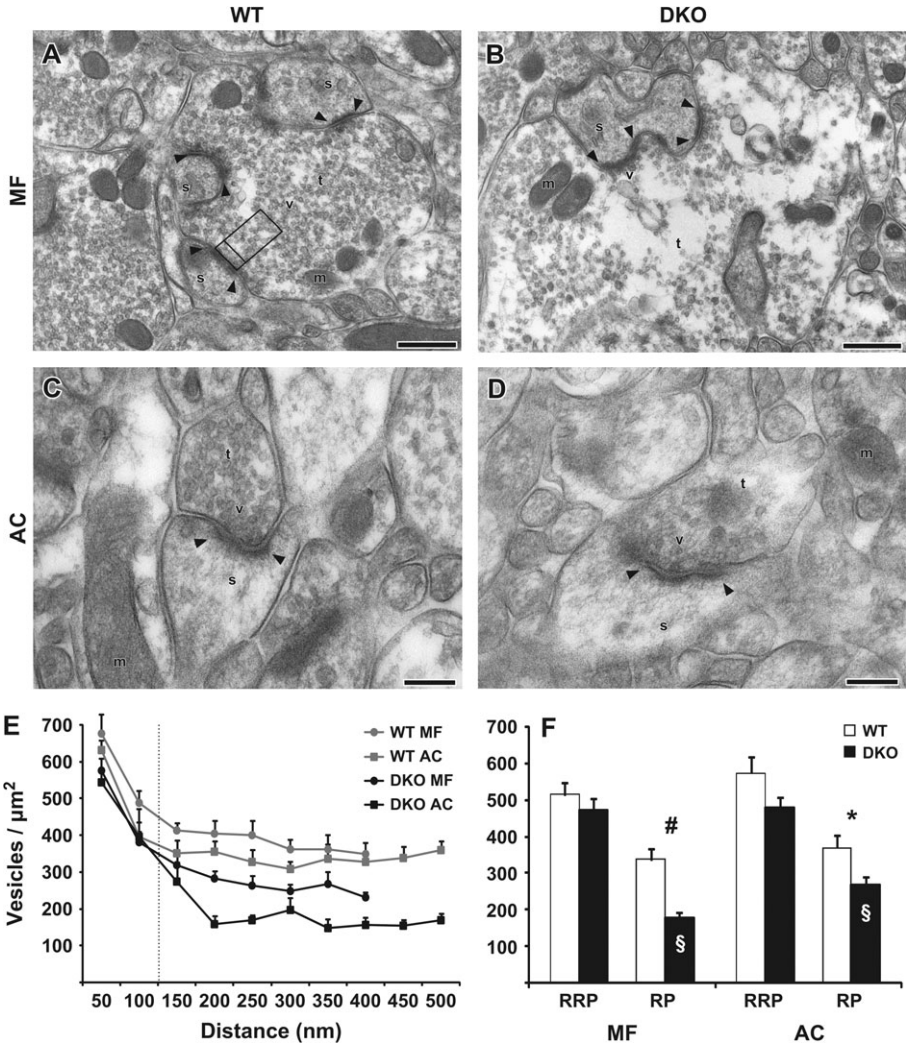

Figure 1. Vesicular densityin MF and AC terminals of synapsin WT and DKO mice. (*A*) Electron micrograph from the CA3 stratum lucidum in the hilus of the area dentata in a perfusion-fixed WT mouse. An MF terminal is marked (t), vesicles (v), mitochondria (m), spines (s) and postsynaptic densities (arrowheads). Opposite of one postsynaptic density, a frame is drawn to illustrate the lateral limits used for counting vesicles in a terminal. Also the distances 0, 100, and 500 nm are marked by lines, representing the categories RRPand RP presented in (*F*). Scale bar: 0.5 µm. (*B*) As in (*A*), but from a synapsin DKO mouse. Vesicular density appears normal close to the synaptic cleft, but severely reduced further away, when compared with (*A*). (*C*) Electron micrograph taken from the CA1 stratum radiatum layer. An AC terminal is marked as in (*A*) (without frame). Scale bar: 0.2 µm. (*D*) As in (*C*), but from a synapsin DKO mouse. The reduction in vesicle density appears less prominent than in B. (*E*) Vesicle densities (mean + standard error of the mean, vesicles/μm^2, $n = 5$ mice) plotted against distance from the synapse in nanometer. Vesicles were grouped in bins of 50 nm and were recorded up to a maximum distance of 500 nm in MF and to 400 nm in AC due to the smaller overall size of AC terminals. The 2 traces from synapsin DKO mice are both below the WT traces. (*F*) As in (*E*), but results are grouped into distances of 0–100-nm distance and 0–400/500 nm, corresponding to RRP and RP, respectively. Symbols indicate differences between means that are statistically significantly different: $^{\#}P = 0.001$, $^{*}P < 0.04$ between WT and DKO, $^{\S}P < 0.01$ between MF and AC. When nonparametric tests were performed, the same groups were statistically different, except between MF and AC (§) which was now at $P = 0.056$. All data are based on 20 electron micrographs (containing 20–46 synapses) from each of 5 perfusion-fixed mice ($n = 5$) per synapse type and genotype.

paraformaldehyde 4% in PBS, and stored at 4 °C overnight. Further, slices were immersed in 0.1 M cacodylate buffer and again incubated overnight at 4 °C. Preparations were washed in 0.1 M cacodylate buffer, treated with 2% aqueous uranyl acetate, dehydrated in ethanol, and embedded in LR Gold (Fluka) at −25 °C.

For both antigens, ultrathin sections were collected on mesh or formvar-coated nickel slot grids and labeled with primary antibodies (actin 20 μg/ml; synapsin 1:400) at 4 °C overnight using the postembedding immunogold technique (Bloom et al. 2003; Bergersen et al. 2008), with secondary antibodies conjugated to 5- (anti-mouse; Amersham Bioscience, Buckinghamshire, UK) or 10-nm gold particles (anti-rabbit; BBI International, Cardiff, UK). When 5 nm gold were used, particles where enhanced using the IntenSE Silver Enhancement kit (Amersham Biosciences). No labeling was observed in sections where primary antibody was omitted. For analyses of synapsin labeling, the average number of gold particles was calculated and compared in 20 terminals per synapse type (AC and MF) from 5 WT and 5 synapsin DKO (the latter representing synapsin III plus background). Terminals were divided into an RRP, 0–100 nm, an RP, 0–400 nm, endocytic zone (EZ), 250 × 150 nm lateral to the sides of the active zone (or less if the terminal was smaller), as well as a total for the whole terminal was calculated. In sections stained with F-actin antibodies, the density of gold particles was quantified from 20 synapses in WT (n = 2) and synapsin DKO (n = 2) animals in the EZ region, the whole terminal and dendrite.

Electrophysiological Analysis

Hippocampal slices from adult WT and synapsin DKO mice were placed in a humidified interface chamber at 28–32 °C and perfused with ACSF containing 2 mM $CaCl_2$. To avoid *N*-methyl D-aspartate receptor–mediated synaptic plasticity, 50 μM AP5 (Sigma–Aldrich, St. Louis, MO) was present in the ACSF throughout all experiments. In experiments where we analyzed the effects of cytochalasin B (20 μM; Sigma–Aldrich), slices were incubated with the drug for at least 90–120 min prior to stimulus trains (Jensen et al. 2007). Orthodromic stimuli (50 μs, <300 μA, 0.1 Hz) were delivered alternately through 2 tungsten electrodes, with one situated in the hilus of the fascia dentata, close to the upper blade of the granule cell layer of the dentate gyrus, and the other situated in the stratum radiatum of the CA3 region. Extracellular synaptic responses were monitored by 2 glass electrodes (filled with ACSF) that were placed in the corresponding synaptic layers, that is, the stratum lucidum and the stratum radiatum of the CA3 region, respectively. After obtaining stable synaptic responses for at least 15 min, we stimulated the MF–CA3 pyramidal cell or the CA3–CA3 recurrent pathways with trains of repetitive stimuli at defined frequencies (0.5 or 2 Hz) for 15 min. The synaptic efficacy was assessed by measuring the peak amplitude of the MF-elicited fEPSP and the radiatum-elicited fEPSP slope (in the middle third of its rising phase). The value of each response was normalized to the mean value recorded prior (1–3 min) to the high-frequency stimulation. Data were pooled across animals of the same genotype. At the end of some of the experiments, addition of the group II mGluR agonist DCG IV (3 μM; Tocris Bioscience, Bristol, UK) led to inhibition of the lucidum-induced fEPSP, demonstrating the specificity of the MF-elicited responses (Nicoll and Schmitz 2005).

Statistics

Values are presented as mean ± standard error of the mean, and statistical significance of differences was evaluated using a Student's 2-tailed unpaired *t*-test. When the mean of more than 2 groups was compared (fig. 3*E, F*), a one-way analysis of variance test was performed, using Scheffe's post hoc test. Additionally, the following nonparametric statistical tests were employed: Mann–Whitney, Kruskal–Wallis (with Dunn's post hoc test), and Wilcoxon (SPSS, Chicago, IL).

Results

Ultrastructure of MF and AC Synapses in WT and Synapsin DKO Mice

The synaptic vesicle densities were quantified on electron micrographs from WT and synapsin DKO mice to determine possible structural effects in the hippocampal MF and AC terminals induced by genetic inactivation of synapsins I + II (Fig. 1). The vesicle densities were quantified in sequential 50-nm-wide zones at increasing distances from the presynaptic membrane specialization (see Materials and Methods). In the synapsin DKO mice, the MF terminals showed a significant reduction in the vesicle densities in areas located at distances more than 100 nm from the presynaptic membrane specialization (Fig. 1*F*), areas which most probably contain vesicles corresponding to the RP of vesicles (Pieribone et al. 1995; Schikorski and Stevens 1997). In contrast, we observed similar vesicle densities at 0- to 100-nm distance from the presynaptic membrane specialization in the 2 genotypes (Fig. 1*F*). Analysis of vesicle densities in AC terminals revealed no overall differences between synapsin DKO and WT control mice in the closely apposed vesicles (0–100 nm) and only minor reductions in those further away from the presynaptic membrane (Fig. 1*F*).

We extended this analysis to hippocampal slices from the 2 genotypes, with special emphasis on MF terminals. Electron micrographs of MF terminals from slices fixed without prior pharmacological or electrophysiological manipulations revealed an unchanged vesicle density in the RRP, whereas a significant reduction in vesicle density manifested itself in the RP (Fig. 2*F*), thus substantiating the findings observed in perfusion-fixed material. Furthermore, stimulation of the slices by high $[KCl]_o$ (30 mM), in order to depolarize all nerve endings, failed to have a major impact on vesicle densities and, in addition, revealed no further differences between the 2 genotypes. Both the similar vesicle density in the presumed RRP and the reduced vesicle densities in the RP of synapsin DKO mice were maintained (Fig. 2*F*).

Intersynaptic Differences in the Levels of Synapsins I + II and Synapsin III Investigated by Immunogold Analysis

In agreement with reports where cultured hippocampal neurons were labeled for synapsin I (Tao-Cheng 2006; Tao-Cheng et al. 2006), our study shows that synapsin labeling in the MF terminals of WT mice was significantly lower in the area close to the presynaptic membrane specialization (0–100 nm) than in the cytoplasmic clusters (>100 nm) (Fig. 3*A, G*). This synapsin distribution was similar to that observed in the WT AC terminals (Fig. 3*B, G*) and was comparable to that seen in synapses from cultured hippocampal neurons incubated under nondepolarizing conditions (Tao-Cheng et al. 2006). In contrast, in preparations from synapsin DKO mice, where no synapsin I or synapsin II immunoreactivity remained, weak synapsin immunolabeling was observed in MF terminals in close apposition to the presynaptic membrane specialization (Fig. 3*E, G*). This distribution was comparable to the synapsin I enrichment in the RRP seen in synapses from cultured hippocampal neurons incubated under depolarizing conditions (Tao-Cheng et al. 2006). Given that synapsin III is specifically expressed in the MF synapses of DKO brains (Pieribone et al. 2002), our data suggest that synapsin III in these MF terminals is associated with the synaptic vesicles enriched in the RRP. The very low labeling at other sites in the synapsin DKO brain attests to the specificity of the antibody used and to the presence of, in general, very low levels of synapsin III outside MF terminals in adult mice (Pieribone et al. 2002).

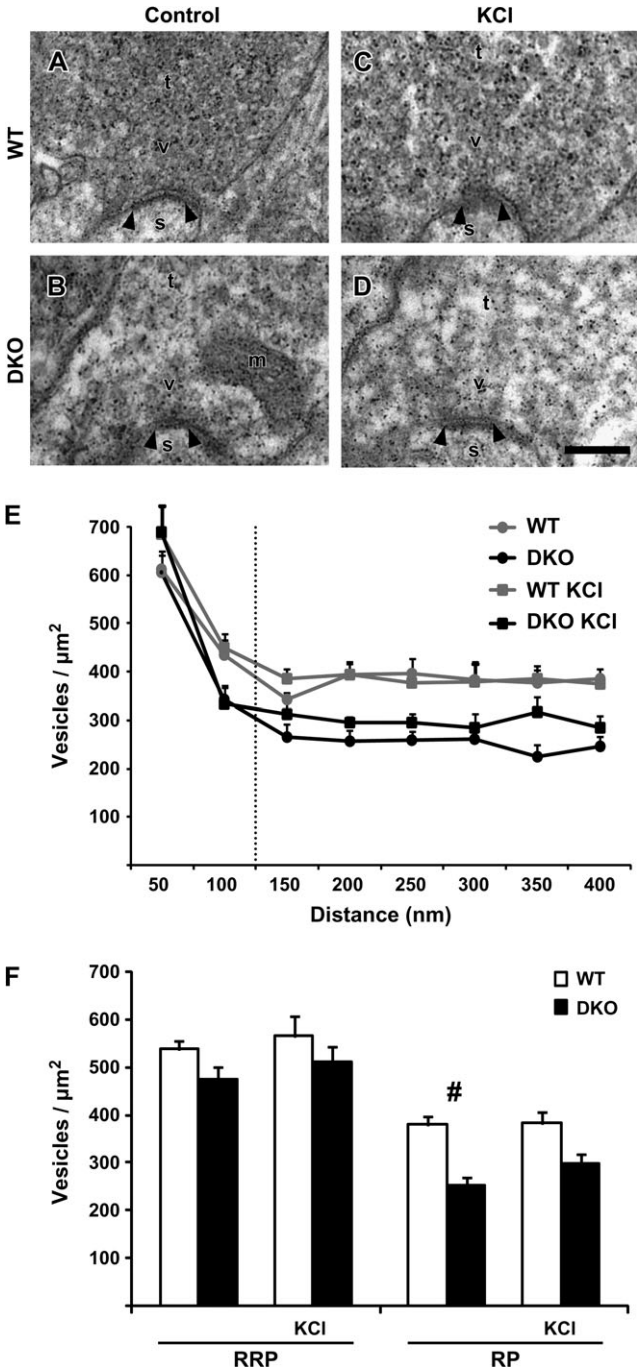

Figure 2. Vesicular density in stimulated and control MF terminals in synapsin WT and DKO mice. (*A*) Electron micrograph of a MF terminal (t) from a WT hippocampal slice preparation. A synapse is indicated by its postsynaptic density (arrowheads), spine (s), vesicles (v), and mitochondria (m). Scale bar: 0.1 µm. (*B*) As in (*A*), but the electron micrograph is from a synapsin DKO MF terminal. (*C*, *D*) As in (*A*) and (*B*), respectively, but the electron micrographs are from slices exposed to 30 mM $[KCl]_o$. Artifactual small, electron-dense precipitates are present in electron micrographs (*A*–*D*). (*E*) Vesicle densities (mean + standard error of the mean, vesicles/µm^2, $n = 3$ mice) plotted against distance from the presynaptic membrane specialization in WT and synapsin DKO mice, either in control situation or exposed to high $[KCl]_o$. Vesicles were grouped into bins of 50 nm and were recorded up to a maximum distance of 400 nm. (*F*) As in (*E*), but results are grouped into distances of 0- to 100-nm distance and 0–400 nm, corresponding to RRP and RP, respectively. Vesicle densities were compared between genotypes at the given distances ($^{\#}P < 0.01$). This could not be confirmed with a Mann–Whitney test because of the low *n*. For each condition, 3 WT and 3 synapsin DKO mice ($n = 3$) were analyzed and compared (20 electromicrographs containing 18–45 synapses were analyzed in each mouse).

F-Actin Immunoreactivity in MF and AC Synapses

Previous studies in lamprey reticulospinal synapses have shown that prolonged depolarization by high $[KCl]_o$ (40 mM for 5–30 min) decreased the size (diameter) and the number of vesicles in the cytoplasmic clusters but not the number of docked vesicles close to the active zone (Wickelgren et al. 1985). This effect resembled the one induced by the injection of synapsin antibodies into reticulospinal axons (Pieribone et al. 1995). Based on these observations, it was suggested that at high stimulation rates vesicles should be recruited from the distal RP of vesicles that appears to be controlled by synapsins (Pieribone et al. 1995). The injection of synapsin antibodies into the reticulospinal axon was found to reduce F-actin polymerization in the EZs surrounding the active zone (Bloom et al. 2003).

To investigate a possible role for actin and synapsin in MF and AC terminals, we investigated the terminals after KCl stimulation. Stable conditions in the slice were ascertained by activating AC fibers through a stimulation electrode placed in stratum radiatum of the CA1 region and monitoring extracellular fEPSPs in the same layer (Fig. 4*A*). After obtaining stable synaptic responses (10–15 min), we raised the extracellular concentration of KCl to 40 mM. This resulted in a delayed increase in the fEPSP responses, followed by a rapid decline in response magnitude. Approximately 3 min after the initial effects of the exposure, a time span during which KCl-induced neurotransmitter release from isolated nerve terminals goes to completion (McMahon and Nicholls 1991), the synaptic responses disappeared completely (Fig. 4*B*). Four minutes after the responses disappeared, the slices were rapidly transferred to fixative solution for subsequent immunocytochemical processing.

Following high $[KCl]_o$ stimulation, MF terminals displayed an approximately 50% reduced level of F-actin immunoreactivity in EZs in synapsin DKO mice compared with WT mice (Fig. 4*C, E, G*). In contrast, no reduction was seen in the AC terminals (Fig. 4*D, F, G*). There was also no general reduction in F-actin in the pre- or postsynaptic compartments of the synapses (Fig. 4*H, I*). Therefore, we suggest that vesicle cycling in the large MF terminals is associated with synapsin-dependent F-actin polymerization.

Frequency Facilitation in MF and AC Synapses

We recorded fEPSPs at MF–CA3 pyramidal cell synapses in the hippocampal slice preparation (Fig. 5*A, B*). These synapses, located on the proximal part of the apical dendrites of CA3 principal cells, show a robust and pronounced short-term synaptic enhancement, in contrast to AC–CA3 pyramidal cell synapses located at the more distal part of the apical dendrites. We first confirmed that, following stable baseline responses at 0.1 Hz, a 2-Hz stimulus train gave a strong frequency facilitation (Salin et al. 1996); this initially led to a 4- to 5-fold response enhancement (Fig. 5*C*), which slowly declined during continuous 2-Hz stimulation. An approximately 3-fold response enhancement was still present after 15 min with this stimulation paradigm. Termination of the 2-Hz train then led to a rapid reversal of response magnitude back to baseline levels (Fig. 5*C*). For comparison, when a similar stimulus train was delivered to the AC fibers in the CA3 stratum radiatum, only an initial, small, and transient facilitation was seen (Fig. 5*F*). The considerable differences between the response patterns

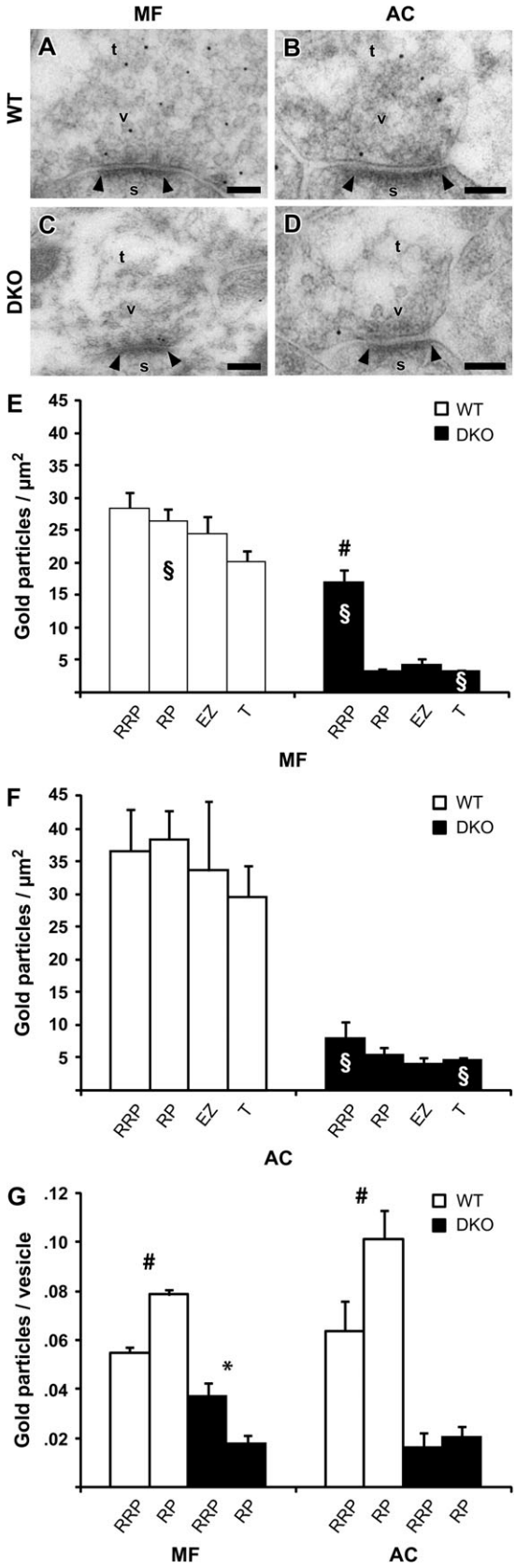

Figure 3. Synapsin Ia/IIa/IIIa panspecific labeling in MF and AC terminals from perfusion-fixed WT and synapsin DKO mice. (*A*) Electron micrograph from a WT MF terminal immunolabeled with synapsin G304 antibodies. A synapse is indicated by its postsynaptic density (arrowheads), spine (s), and vesicles (v). Gold particles were quantified within an RRP and RP zone, morphologically defined according to distances from the presynaptic membrane, 0–100 nm and 100–400 nm, respectively, and laterally limited by a line drawn perpendicularly to the synaptic cleft (see Fig. 1). EZs were defined to be 150 × 250 nm lateral to the RRP or less for smaller synapses. Averages for whole terminals where also acquired (T). Scale bar: 0.1 µm. (*B*) As in (*A*), but the electron micrograph is from an AC terminal in a WT mouse. (*C*, *D*) As in (*A*) and (*B*), but the electron micrographs are from a synapsin DKO mouse. Notice that the only prominent labeling is in the RRP of MF, probably representing synapsin III. (*E*, *F*) Histograms showing a comparison between quantified data obtained from 5 WT and 5 DKO mice, in MF, (*E*), and AC, (*F*). In DKO, the RRP was significantly different from all other areas, and by several orders of magnitude, indicative of the presence of synapsin III. Also, this could explain the unexpectedly dense labeling in the WT RRP. (*G*) As in (*E*) and (*F*), but average gold particle density is combined with average vesicle density from Figure 1 to correct for error due to variations in vesicle density. In (*E*) and (*F*), labeling is artificially high in the RRP due to high vesicle density. Still, a difference between RRP and RP in DKO MF terminals can be seen. Twenty images where analyzed in each of 5 mice ($n = 5$) per genotype and type of synapse (containing 17–21 synapses). The columns represent mean + standard error of the mean of gold particles/µm^2 in the specified areas and in the rest of the terminal (T). Densities were compared between the areas using an analysis of variance test with a Scheffe's post hoc test ($^{\#}P < 0.01$) and between DKO and WT using the *t*-test ($^{\S}P < 0.04$). A Kruskal–Wallis and Mann–Whitney tests gave similar results ($P < 0.05$).

argue that the 2 pathways were selectively activated with this experimental design, with relatively little cross-contamination. This was further supported by the effect of the mGluR II agonist DCG IV (3 µM) (Nicoll and Schmitz 2005), which selectively abolished the stratum lucidum response (data not shown).

We next examined the functional importance of synapsins I and II during stimulus trains at the MF–CA3 synapse. Application of stimulus trains at 0.5-Hz frequency resulted in similar response patterns and magnitudes in the 2 genotypes. Neither the pooled maximum magnitude (normalized to baseline, WT: 1.83 ± 0.15, $n = 16$ slices from 7 animals; DKO: 1.76 ± 0.13, $n = 14$ slices from 6 animals) nor the time needed to reach the maximum magnitude (WT: 41.5 ± 8.1 s; DKO: 39.6 ± 5.7 s) was different in the 2 genotypes (Fig. 5*E*). Thus, at this low stimulation frequency, the MF-specific response enhancement appeared not to involve synapsin-dependent vesicle recruitment mechanisms.

A greater facilitation was obtained when 2-Hz stimulus trains were delivered, a frequency that is within the physiological firing range of granule cells (Mori et al. 2004; Bischofberger et al. 2006). In contrast to 0.5-Hz stimulation, the degree of facilitation was greater in WT than synapsin DKO mice (Fig. 5*D*), peaking at 4.47 ± 0.69 ($n = 16$ slices from 9 animals) and 2.47 ± 0.33 ($n = 15$ slices from 8 animals) relative magnitudes, respectively. The time needed to reach the maximum magnitude (WT: 33.7 ± 4.2 s; DKO: 28.7 ± 3.7 s) was similar in the 2 genotypes. These results suggest that 0.5-Hz stimulation involves synapsin I + II–independent recruitment of vesicles into the releasable vesicle pool, whereas 2-Hz stimulation involves an additional recruitment that depends on the presence of synapsins I + II.

In contrast to the striking differences at the MF synapses, the AC collateral synapses in CA3 behaved similarly in synapsin DKO and WT mice, although the frequency facilitation at 2-Hz stimulation tended to be more pronounced in synapsin DKO than in WT mice (Fig. 5*G*), similar to what has been observed at the CA3-to-CA1 radiatum synapses in the CA1 region (Hvalby et al. 2006). Statistical evaluation, however, failed to reveal a difference in both the pooled maximum magnitude

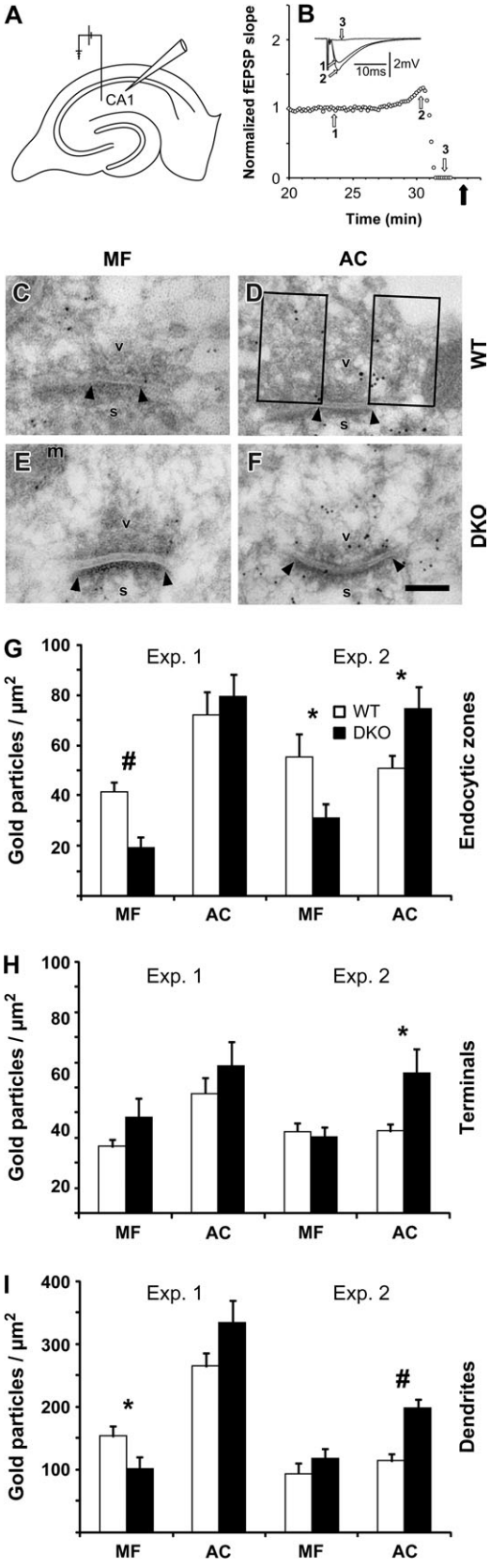

Figure 4. F-actin labeling in AC and MF terminals in WT and synapsin DKO mice exposed to depolarizing $[KCl]_o$. (*A*) Schematic drawing of a hippocampal slice with the electrode arrangements in stratum radiatum of the CA1 region. (*B*) The graph shows an example of the change in fEPSP slope as a function of time when a WT slice is incubated in high $[KCl]_o$ (40 mM). Afferent stimulation and synaptic recordings are as depicted in (*A*). The slopes of the elicited fEPSPs were normalized to the mean value obtained 1 min prior to the start of high $[KCl]_o$ wash-in (time zero), and the effects are presented from around 27 min and onward. Filled arrow indicates the time at which the slice was removed from the recording chamber and fixed. Inset: superimposed synaptic responses at times indicated by open arrows and numbers. (*C*) Electron micrograph from a MF terminal exposed to high $[KCl]_o$ in a hippocampal slice from a WT mouse. A synapse is indicated by its postsynaptic density (arrowheads), spine (s), vesicles (v), and mitochondria (m). Scale bar: 0.1 µm. (*D*) As in (*C*), but the electron micrograph is from an AC collateral terminal. Boxes represent the EZs analyzed (150 nm lateral to the active zone and 250 nm perpendicular to the active zone, unless further restricted by the size of the terminal). (*E*, *F*) As in (*C*) and (*D*), but from synapsin DKO mice. (*G*) Bar graph (mean + standard error of the mean) representing quantitative analyses of F-actin in EZs (gold particles/µm^2). Two pairs of WT and synapsin DKO mice were analyzed independently and repeated once (experiments 1 and 2). Twenty electron micrographs (containing 25–33 synapses) were analyzed for each synapse type in each animal. Actin-labeling densities were compared between genotypes. A prominent reduction in DKO compared with WT was observed in MF EZ only, in both experiments ($^{\#}P \leq 0.002$, $^{*}P \leq 0.03$). The nonparametric Mann–Whitney test gave similar results. (*H*) As in (*G*), but quantified in the whole terminal. No differences were observed in either experiment. (*I*) As in (*G*), but quantified in the dendrites postsynaptic to terminals in (*G*) and (*H*) (different scale due to a generally more dense labeling than in *G* and *H*). No differences were observed.

(normalized to baseline, WT: 1.18 ± 0.06, n = 15 slices from 8 animals; DKO: 1.21 ± 0.03, n = 17 mice from 9 animals) and in the time needed to reach the maximum magnitude (WT: 11.4 ± 2.1 s; DKO: 12.0 ± 1.4 s). At 0.5-Hz stimulation, hardly any frequency facilitation was present and both the pooled maximum magnitude (WT: 1.05 ± 0.03, n = 13 slices from 6 animals; DKO: 1.12 ± 0.02, n = 16) and the time to the peak of the facilitation (WT: 33.2 ± 7.8 s; DKO: 29.9 ± 5.3 s) were similar in the 2 genotypes (Fig. 5*H*).

Modulation of F-Actin Induces Changes in Ultrastructure and Frequency Facilitation

In order to evaluate the physiological significance of the reduced level of F-actin immunoreactivity in EZs of MF terminals in synapsin DKO mice, we examined possible changes in ultrastructure and synaptic transmission following severing of actin filaments. Preincubation of the slices with cytochalasin B (20 µM) (Cooper, 1987) for 120 min with 0.017-Hz stimulus frequency induced a decrease in baseline responses of similar magnitude in the 2 genotypes both at the MF–CA3 synapses (WT [peak fEPSP amplitude]: 0.80 ± 0.08, n = 10, 4 animals; synapsin DKO: 0.80 ± 0.06, n = 20, 5 animals) and at the AC collateral–CA3 synapses (WT [fEPSP slope]: 0.75 ± 0.10, n = 12, 3 animals; synapsin DKO: 0.78 ± 0.05, n = 11, 3 animals). The effect in the present experiments is almost identical to the ones earlier observed in radiatum synapses of the CA1 region (Kim and Lisman, 1999; Jensen et al. 2007). The treatment had no effect on the MF vesicle density at 0–50 nm from the presynaptic membrane specialization but reversed the reduction in vesicle density in the presumed cytoplasmic RP at 100–400 nm in the synapsin DKO genotype. Moreover, this effect of F-actin destabilization on preparations from the synapsin DKO animals occurred both in KCl-stimulated and in -unstimulated preparations (Fig. 6*A*–*F*).

Application of 2-Hz trains to the MFs in the presence of cytochalasin B again evoked considerable enhancement of fEPSPs. However, the degree of enhancement was now similar in the 2 genotypes (WT: 3.14 ± 0.31, n = 16; synapsin DKO: 2.65 ± 0.40, n = 17) and comparable to the degree of enhancement seen in synapsin DKO mice without cytochalasin

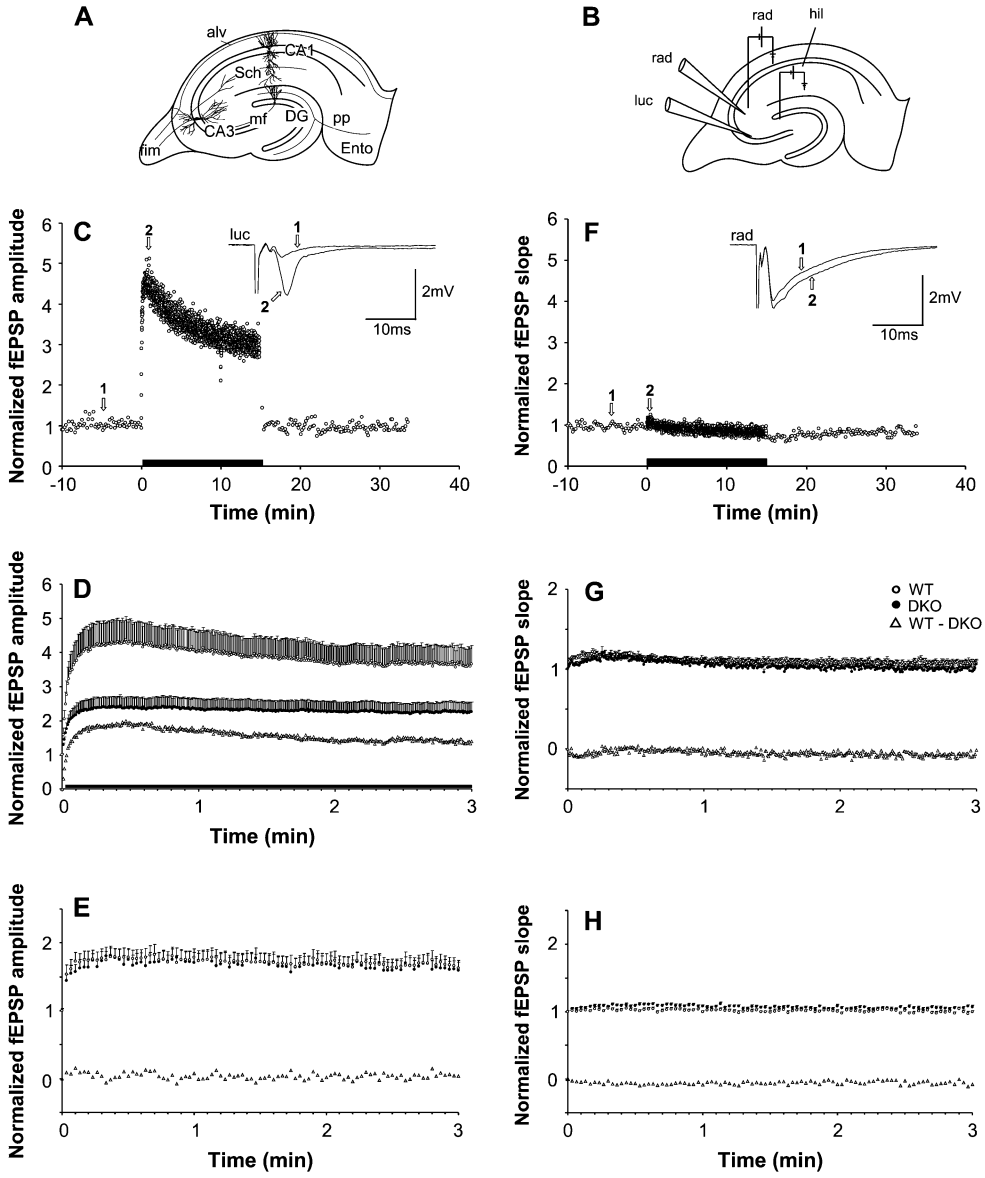

Figure 5. Frequency facilitation in the MF–CA3 and AC collateral–CA3 pathways. (*A*) Schematic drawing of the hippocampal slice with a simplified relevant excitatory network. Ento, entorhinal cortex; DG, dentate gyrus, pp, perforant path; fim, fimbria; alv, alveus; Sch, Schaffer collaterals (branches of AC collateral axons). (*B*) Schematic drawing showing electrode arrangement in the CA3 region. One recording electrode was placed extracellularly in stratum lucidum (luc), the other in stratum radiatum (rad) in order to monitor synaptic responses elicited by stimulation electrodes placed in the hilus (hil) and in the stratum radiatum for selective stimulation of MFs and AC collaterals, respectively. (*C*) Normalized fEPSP amplitude measurements during afferent stimulation of the MF in an experiment at 0.1 Hz in WT mice, followed by 2 Hz for 15 min (indicated by black bar along the abscissa), and reversal to 0.1 Hz. Inset shows the mean of 5 consecutive responses at times indicated by open arrows and numbers. (*D*) Normalized and pooled MF-elicited fEPSPs in WT (open circles) and synapsin DKO (filled circles) mice following the switch from 0.1- to 2-Hz stimulation (only the first 3 min are shown). Subtraction of the values obtained in synapsin DKO mice from those obtained in WT mice is represented by the open triangles. Vertical bars indicate standard error of the mean. Black horizontal bar along the abscissa indicates that the genotypes differ ($P < 0.05$). (*E*) As in (*D*), but following the switch from 0.1- to 0.5-Hz stimulation of the MF–CA3 pathway. (*F*) as in (*C*) and (*G*) and (*H*) as in (*D*) and (*E*), but measurements are from responses elicited by stimulation of the AC collateral–CA3 pathway.

B (Fig. 6*G*). These results imply that those synaptic vesicles in MF terminals that can be recruited to the releasable pool in a synapsin I + II–dependent manner are also dependent on F-actin filaments, whereas the vesicles recruited independently of synapsins I + II are not.

At the AC collateral–CA3 synapses, 2-Hz trains in the presence of cytochalasin B elicited a similar amount of frequency facilitation in both genotypes (WT: 1.15 ± 0.07, n = 15, 3 animals; synapsin DKO: 1.22 ± 0.07, n = 12, 3 animals) and not significantly different from what was observed in normal solution (see above). In these small presynaptic boutons, F-actin filaments do not appear to contribute to the frequency facilitation observed at 2-Hz stimulation.

Discussion

Distinct types of presynaptic plasticity depend on a limited number of molecular, structural, and functional factors, including the synapsin protein family (e.g., Hilfiker et al. 1999; Atwood and Karunanithi 2002). Previous studies indicated that the MF-to-CA3 pyramid synapses in the hippocampus displayed major structural changes but retained functional characteristics

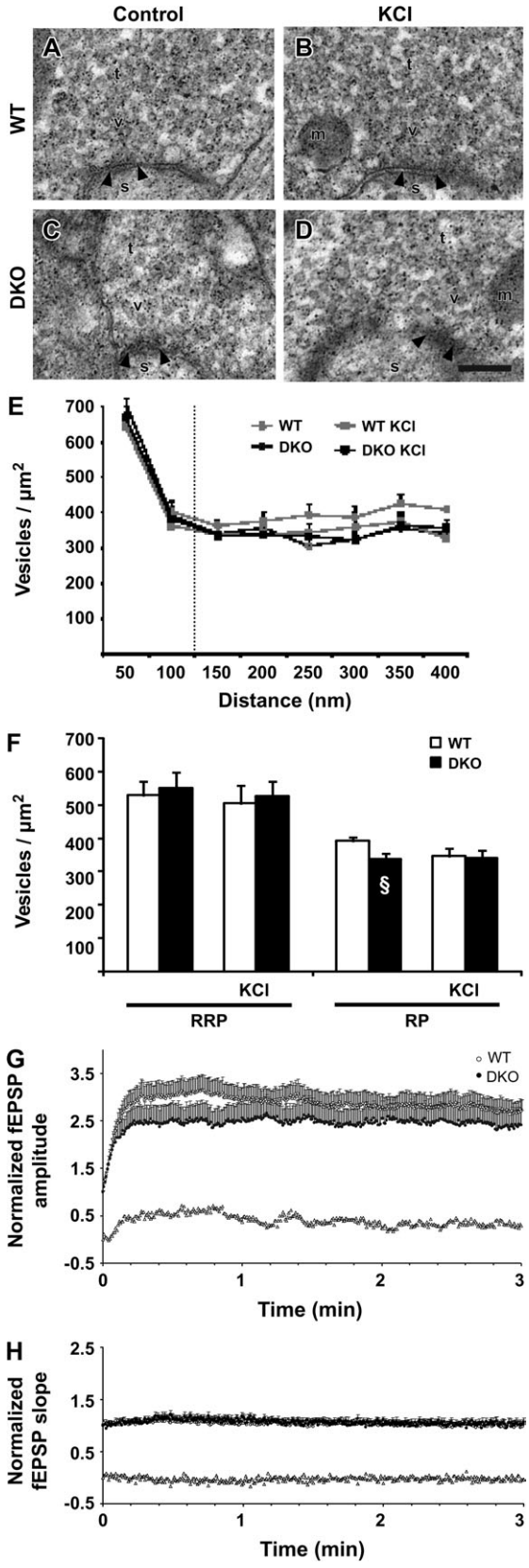

Figure 6. Effects of F-actin modulation on vesicle densities and frequency facilitation at MF–CA3 synapses in slices. (*A*) Electron micrograph from a control WT MF terminal (t) exposed to cytochalasin B (20 μM). The synapse is indicated by its postsynaptic density (arrowheads), spine (s), vesicles (v), and mitochondria (m). Scale bar: 0.1 μm. (*B*) As in (*A*), but the electron micrograph is from a WT MF terminal which subsequently to cytochalasin B (20 μM) exposure was stimulated with 30 mM $[KCl]_o$. (*C*, *D*) As in (*A*) and (*B*), but the electron micrographs are from synapsin DKO MF terminals. Artifactual small, electron-dense precipitates are present in electron micrographs (*A*–*D*). (*E*) Bar graph (mean + standard error of the mean [SEM]) showing the vesicle densities (vesicles/μm^2) at increasing distance from the presynaptic membrane specialization in both genotypes in control situation and exposed to high $[KCl]_o$. (*F*) Bar graph results are grouped into distances of 0- to 100-nm distance and 0–400 nm, corresponding to RRP and RP, respectively. Vesicle densities were compared between genotypes at the given distances and no differences found. For each of the treatments, 3 WT and 3 synapsin DKO mice (the number of synapses in each animal ranged from 18 to 34 in 20 electron micrographs from each slice). Note the increase in DKO vesicle density, rather than a decrease in WT. $^{\S}P < 0.05$ between DKO with and without cytochalasin B when comparing Figure 2*F*. (*G*) Normalized and pooled MF-elicited fEPSPs in WT (open circles) and synapsin DKO (filled circles) mice following the switch from 0.1- to 2-Hz stimulation (only the first 3 min are shown) in the presence of cytochalasin B (20 μM). Subtraction of the values obtained in synapsin DKO mice from those obtained in WT mice is represented by the open triangles. Vertical bars indicate SEM. (*H*) As in (*F*), but measurements are from responses elicited by stimulation of the AC collateral–CA3 pathway in the presence of cytochalasin B (20 μM).

following genetic ablation of synapsins I and/or II (Spillane et al. 1995; Takei et al. 1995). There may, however, be diversity among different nerve terminals. Thus, retinogeniculate terminals seem to lack these synapsins (Kielland et al. 2006), and there are divergent reports on the effect of perturbation of actin in distinct preparations of cultured hippocampal neurons (Ryan et al. 1996; Sankaranarayanan et al. 2003; Darcy et al. 2006). Synaptic activity is associated with the formation of actin filaments at the periactive zone (Bloom et al. 2003). The resulting scaffold may be more important in large than in small terminals. The MF synapses are unique by their large size and wide dynamic range of firing. The present study reports novel aspects of structure and function that are highly regulated by synapsins I + II and actin filaments in these giant excitatory terminals, compared with AC terminals, the major class of small excitatory terminals in the region.

Reduction of Vesicle Density in the RP of Synapsin DKO Mice

In the MF terminals, the density of vesicles in synapsin DKO mice is significantly reduced within areas farther than 100 nm away from the active zone of the presynaptic terminal, that is, in the RP of synaptic vesicles (Pieribone et al. 1995; Ashton and Ushkaryov 2005). A similarly pronounced reduction was not seen in the terminals of the AC collaterals, suggesting that in this regard the MF synapses are distinct from AC terminals.

The stability of the cytoplasmic vesicle clusters may primarily depend on synapsin-mediated associations between the synaptic vesicles within the clusters (Pieribone et al. 1995). Hence, in terminals devoid of synapsins I + II, the cytoplasmic vesicle clusters would be expected to be decreased in size, vesicle numbers, or vesicle densities. Our data agree with this prediction. As the effect was observed in acute brain slices as well as in tissue that was perfusion fixed under deep barbiturate anesthesia, it is presumably present in basal conditions. There was no further reduction in the cytoplasmic cluster of vesicles upon potassium stimulation, suggesting that the endocytic recovery of vesicles is keeping pace with exocytosis under these conditions.

Strong frequency facilitation is known to occur in the MF during prolonged stimulus trains at both 0.5- and 2-Hz stimulation frequencies (Salin et al. 1996), probably reflecting,

at least in part, the mobilization and translocation of synaptic vesicles from the cytoplasmic vesicle clusters into the RRP. Our data suggest that this frequency facilitation derives from 2 distinct pools, based on the observation that the major part of the facilitation, representing approximately 60% of the maximal response at 2 Hz, was not seen in the synapsin DKO and, therefore, must represent vesicles recruited to the releasable pool by a synapsin I + II–dependent mechanism. Interestingly, this part of the frequency facilitation, previously not described, also depends on the presence of F-actin filaments because interfering with either synapsin or F-actin occluded the response in a similar fashion. Thus, our data suggest that these proteins may share mechanisms of action during frequency facilitation.

These data are in general agreement with previous studies on vesicle clusters, most of which indicate that the clusters are stabilized by synapsin cross-linking vesicles (Pieribone et al. 1995; Awizio et al. 2007), whereas vesicle mobilization processes require cycling of actin microfilaments (Sakaba and Neher 2003; Ashton and Ushkaryov 2005; Jensen et al. 2007). In contrast, the synapsin-independent part of the frequency facilitation occurring in the synapsin DKO at 2 Hz, which represented approximately 40% of the maximum response enhancement occurring in the WT, was not sensitive to F-actin depolymerization. This latter response pattern may rather represent equilibrium between vesicle recruitment and exocytosis that does not involve synapsin- or actin-dependent recruitment mechanisms.

Our study also indicates that the synaptic response enhancement that is dependent on synapsin and F-actin is transient, since after the peak occurring at 30 s, the fEPSP decreased steadily for at least 15 min. Interestingly, activity of MFs at different frequencies entrains distinct network consequences: low-frequency stimulation of granule cells induces MF-mediated synaptic inhibition of target CA3 cells, whereas high-frequency stimulations induce monosynaptic excitatory CA3 pyramidal cell responses (Mori et al. 2004). The differential recruitment of these pathways possibly reflects distinct patterns of frequency-dependent facilitation at giant MF synapses, which terminate on pyramidal neurons, whereas small synapses made by filopodia-like extensions terminate on inhibitory interneurons in CA3 (Acsady et al. 1998).

In contrast to the MF synapse, the small AC collateral synapse located on more distal parts of CA3 pyramidal cell apical dendrites did not respond to similar stimulus trains with strong frequency facilitation. Correspondingly, AC collateral synapses showed only minor changes in the synapsin DKO mice, further emphasizing the differences between the giant MF and the small AC terminals.

Moreover, following KCl treatment of slices, F-actin immunoreactivity at the periactive zones, where endocytosis takes place, was significantly reduced in the MF synapses in the synapsin DKO compared with WT. No such reduction occurred in the AC synapses. Hence, F-actin and synapsin interaction may be more important during recycling of synaptic vesicles in the giant MF synapse than in the small AC synapse. Stimulus-induced frequency facilitation occurring at 2 Hz in the CA3-to-CA1 AC synapse is negatively regulated by synapsins I + II (Hvalby et al. 2006). In the CA3-to-CA3 AC synapse examined here, the small frequency facilitation observed showed a brief, transient constraining effect of synapsins I + II. This is in stark contrast to the synapsin-dependent facilitation at the MF synapse, indicating a major difference in functional organization between these synapses.

Stimulation-induced changes in morphology were searched for in slices exposed to a high extracellular potassium concentration. In the WT, no effects on cytoplasmic vesicle clusters were seen after prolonged KCl treatment. This suggests that this synapse has a very efficient mechanism for synaptic vesicle recycling. A similar phenomenon was observed in synapses established by primary afferents in the lamprey spinal cord that display tonic firing pattern and that contain more synapsin per synaptic vesicle than reticulospinal synapses (Evergren et al. 2006).

Because our results suggest that the frequency facilitation at low-to-moderate firing frequencies that appears to be a unique feature of the MF–CA3 synapse is synapsin and actin dependent, this type of frequency facilitation may reflect the mobilization of synaptic vesicles from the RP to the RRP. In contrast, the AC synapses terminating onto CA1 (Jensen et al. 2007) and CA3 pyramidal cells do not show this form of plasticity. This is in line with recent observations indicating that excitatory synapses onto CA1 pyramidal cells, during stimulation at increased frequency are largely dependent on fast refilling of synaptic vesicles, rather than mobilization of reserve vesicles (Ertunc et al. 2007). Of special interest are the frequency-dependent responses on the MF synapses. Although the prevailing physiologic firing frequency of MF is around 0.5–4 Hz, the large size of the vesicle clusters in the MF terminals suggests that these terminals should be able to respond to high-frequency stimulations. In agreement, the firing frequency of MF can increase to >40 Hz when place cells in the dentate area become activated by spatial coordinates (Mori et al. 2004), suggesting that these represent conditions in which vesicles are recruited from the large RP in the MF.

F-Actin Destabilization Normalizes the RP of Vesicles in Synapsin I + II–Deficient MF Terminals

Treatment of synapsin DKO slices with cytochalasin B abolished the reduction in cytoplasmic synaptic vesicle density that has been reported in synapsin-deficient MF terminals (Takei et al. 1995 and this study). Moreover, this effect was due to an increase in vesicle density back to normal levels in the synapsin DKO and not to a decrease in vesicle density in the WT. Hence, we suggest that the decrease in synaptic vesicle density following synapsin I + II perturbations (Rosahl et al. 1995; Gitler et al. 2004; Bogen et al. 2006) may be F-actin dependent. Because recent studies show that synaptic vesicles may migrate between individual hippocampal boutons in an actin-dependent manner (Darcy et al. 2006), it appears probable that increased vesicle mobility caused by the absence of synapsins may be counteracted by destabilizing actin. Interestingly, the increase of cytoplasmic synaptic vesicle clusters in the synapsin DKO terminals after cytochalasin B treatment did not rescue the lost synapsin-dependent frequency facilitation. This suggests that at the physiological 2-Hz frequency, synapsin proteins are required to support vesicle recruitment from cytoplasmic vesicle clusters into the releasable vesicle pool, irrespective of the number of vesicles available in the RP.

Lack of Decrease in Vesicle Density in the AC Terminals

Whereas we found only minor changes in AC terminals, substantial reductions in the number of synaptic vesicles, both

in the cytoplasmic region and in areas close to the presynaptic membrane of AC terminals, have been described earlier in studies of synapsin DKO mice (Rosahl et al. 1995). Recently, major decreases restricted to the cytoplasmic vesicle clusters were reported in a study using high-pressure freezing and cryosubstitution of CA1 slices from synapsin I + II + III triple knockout mice (Siksou et al. 2007). The recent finding that a phosphoprotein different from synapsins regulates vesicle recycling (Gaffield and Betz 2007) may contribute to discrepancies between studies on synapsin knockout. To what extent these discrepancies could be due to different experimental setup, including possible differences in the genetic background of the knockout mice, remains unknown. Because our experiments gave highly reproducible observations of reduced MF vesicle density in the synapsin DKO compared with WT preparations, they cannot be ascribed to random preparation artifacts. The important point is that the changes are larger in MF, indicative of a higher synapsin I + II dependence of the cytoplasmic pool of vesicles in the MF terminals compared with AC terminals.

Synapsin III Localization

It remains possible that the selective decrease of synaptic vesicles seen in the MF terminals could be related to the selective expression of synapsin III in the granule cells and their axons (Pieribone et al. 2002; Kao et al. 2008). Whereas synapsins I and II in adult animals are relatively uniformly distributed among different classes of nerve endings, synapsin III shows a highly restricted distribution, being present in inter alia the MF, where the content of synapsin III remains unchanged in the synapsins I + II DKO mice (Pieribone et al. 2002). Given the restrictive effect of synapsin III on the size of the recycling pool of synaptic vesicles (Feng et al. 2002) in the absence of synapsins I and II, the presence of synapsin III may partly explain the observed reduction of the RP of vesicles in MF. Moreover, the association of synapsin III with the RRP vesicle in MF that we observe may possibly underlie the ability of synapsin III to promote the response depression induced by high-frequency stimulation and the reduction of mEPSP size (Feng et al. 2002). Taken together, these effects could contribute to the unique dynamic range of the MF synapse and the loss of frequency facilitation in synapsin I + II DKO.

In studies of the localization of synapsin III, it has been shown that synapsin III antibodies labels strongly distinct areas within the brain. In mouse hippocampus, the most intense synapsin III labeling is confined to the subgranular layer of area dentata, extending into the hilus and covering a region rich in MF terminals (Pieribone et al. 2002). In the same study, the authors propose that synapsin III is concentrated over vesicle clusters in MF terminals. Also, the same article shows that labeling with synapsin panspecific G304 antibody, the same antibody used in this article, on synapsin I + II DKO mice gives identical staining pattern as if WT mice is stained using synapsin III antibody. Our findings, using electron microscopy, that synapsin III is enriched in the RRP, add to what has previously been reported. In the synapsin DKO mice where the synapsin III labeling is demonstrated, there are a reduced number of vesicles in the clusters; hence, we cannot rule out the theory proposed by Pieribone et al. (2002) that synapsin III is found in vesicle clusters. However, we have analyzed a total of 100 MF terminals in 5 DKO mice without seeing much synapsin III labeling in the RP. In contrast, the labeling in the RRP was significantly enriched compared with RP, also when it was corrected for vesicle density (Fig. 3*G*). Based on these findings, it appears possible that synapsin III could have a specific functional role restricted to the RRP of MF terminals.

In conclusion, our study demonstrates that the regulation of the synaptic vesicle cycle in the giant MF synapse is dependent on synapsins I + II and F-actin. Trafficking of vesicles in AC synapses is less dependent on synapsins and actin. This further supports the idea that different mechanisms may control the cycling of vesicles in synapses established by different populations of neurons in the CNS and in synapses displaying different structural and functional properties. In addition, we show that synapsin III has a highly specific localization in MF terminals, possibly contributing to the unique properties of these synapses.

Funding

The Norwegian Research Council; the Swedish Research Council (grant 13473-06A to OS).

Notes

We thank Dr P. Greengard (The Rockefeller University, New York) and Dr H. T. Kao (Brown Universtiy, Providence, RI) for the gift of synapsin knockout mice and for synapsin G304 antibody. *Conflict of Interest*: None declared.

Address correspondence to email: l.h.bergersen@medisin.uio.no.

References

Acsady L, Kamondi A, Sik A, Freund T, Buzsaki G. 1998. GABAergic cells are the major postsynaptic targets of mossy fibers in the rat hippocampus. J Neurosci. 18:3386–3403.

Ashton AC, Ushkaryov YA. 2005. Properties of synaptic vesicle pools in mature central nerve terminals. J Biol Chem. 280:37278–37288.

Atwood HL, Karunanithi S. 2002. Diversification of synaptic strength: presynaptic elements. Nat Rev Neurosci. 3:497–516.

Awizio AK, Onofri F, Benfenati F, Bonaccurso E. 2007. Influence of synapsin I on synaptic vesicles: an analysis by force-volume-mode of the atomic force microscope and dynamic light scattering. Biophys J. 93:1051–1060.

Bahler M, Greengard P. 1987. Synapsin I bundles F-actin in a phosphorylation-dependent manner. Nature. 326:704–707.

Benfenati F, Bahler M, Jahn R, Greengard P. 1989. Interactions of synapsin I with small synaptic vesicles: distinct sites in synapsin I bind to vesicle phospholipids and vesicle proteins. J Cell Biol. 108:1863–1872.

Bergersen L, Waerhaug O, Helm J, Thomas M, Laake P, Davies AJ, Wilson MC, Halestrap AP, Ottersen OP. 2001. A novel postsynaptic density protein: the monocarboxylate transporter MCT2 is co-localized with delta-glutamate receptors in postsynaptic densities of parallel fiber-Purkinje cell synapses. Exp Brain Res. 136:523–534.

Bergersen LH, Storm-Mathisen J, Gundersen V. 2008. Immunogold quantification of amino acids and proteins in complex subcellular compartments. Nat Protoc. 3:144–152.

Bischofberger J, Engel D, Frotscher M, Jonas P. 2006. Timing and efficacy of transmitter release at mossy fiber synapses in the hippocampal network. Pflugers Arch. 453:361–372.

Blackstad TW. 1956. Commissural connections of the hippocampal region in the rat, with special reference to their mode of termination. J Comp Neurol. 105:417–537.

Blackstad TW, Kjærheim A. 1961. Special axo-dendritic synapses in the hippocampal cortex: electron and light microscopic studies on the layer of mossy fibers. J Comp Neurol. 117:133–159.

Bloom O, Evergren E, Tomilin N, Kjaerulff O, Low P, Brodin L, Pieribone VA, Greengard P, Shupliakov O. 2003. Colocalization of synapsin and actin during synaptic vesicle recycling. J Cell Biol. 161:737–747.

Bogen IL, Boulland JL, Mariussen E, Wright MS, Fonnum F, Kao HT, Walaas SI. 2006. Absence of synapsin I and II is accompanied by decreases in vesicular transport of specific neurotransmitters. J Neurochem. 96:1458–1466.

Chicurel ME, Harris KM. 1992. Three-dimensional analysis of the structure and composition of CA3 branched dendritic spines and their synaptic relationships with mossy fiber boutons in the rat hippocampus. J Comp Neurol. 325:169–182.

Cooper JA. 1987. Effects of cytochalasin and phalloidin on actin. J Cell Biol. 105:1473–1478.

Darcy KJ, Staras K, Collinson LM, Goda Y. 2006. Constitutive sharing of recycling synaptic vesicles between presynaptic boutons. Nat Neurosci. 9:315–321.

Delgado R, Maureira C, Oliva C, Kidokoro Y, Labarca P. 2000. Size of vesicle pools, rates of mobilization, and recycling at neuromuscular synapses of a Drosophila mutant, shibire. Neuron. 28:941–953.

Dobrunz LE, Stevens CF. 1997. Heterogeneity of release probability, facilitation, and depletion at central synapses. Neuron. 18:995–1008.

Ertunc M, Sara Y, Chung C, Atasoy D, Virmani T, Kavalali ET. 2007. Fast synaptic vesicle reuse slows the rate of synaptic depression in the CA1 region of hippocampus. J Neurosci. 27:341–354.

Evergren E, Benfenati F, Shupliakov O. 2007. The synapsin cycle: a view from the synaptic endocytic zone. J Neurosci Res. 85:2648–2656.

Evergren E, Zotova E, Brodin L, Shupliakov O. 2006. Differential efficiency of the endocytic machinery in tonic and phasic synapses. Neuroscience. 141:123–131.

Feng J, Chi P, Blanpied TA, Xu Y, Magarinos AM, Ferreira A, Takahashi RH, Kao HT, McEwen BS, Ryan TA, et al. 2002. Regulation of neurotransmitter release by synapsin III. J Neurosci. 22:4372–4380.

Ferreira A, Chin LS, Li L, Lanier LM, Kosik KS, Greengard P. 1998. Distinct roles of synapsin I and synapsin II during neuronal development. Mol Med. 4:22–28.

Gaffield MA, Betz WJ. 2007. Synaptic vesicle mobility in mouse motor nerve terminals with and without synapsin. J Neurosci. 27(50):13691–13700.

Gitler D, Takagishi Y, Feng J, Ren Y, Rodriguiz RM, Wetsel WC, Greengard P, Augustine GJ. 2004. Different presynaptic roles of synapsins at excitatory and inhibitory synapses. J Neurosci. 24:11368–11380.

Greengard P, Valtorta F, Czernik AJ, Benfenati F. 1993. Synaptic vesicle phosphoproteins and regulation of synaptic function. Science. 259:780–785.

Gylterud Owe S, Jensen V, Hvalby O, Evergren E, Shupliakov O, Walaas SI, Storm-Mathisen J, Bergersen LH. 2007. Distribution of vesicles in mossy fiber hippocampal synapses after perturbation of actin and synapsin. Program No. POS-MON-116. Abstract Viewer/Itinerary Planner [Internet]. Melbourne (Australia): International Brain Research Organisation.

Gylterud S, Shupliakov O, Walaas SI, Storm-Mathisen J, Bergersen LH. 2004. Disruption of vesicle clusters in glutamatergic terminals in the hippocampus of synapsin I/II-deficient mice. Program No. 967.8. In: Abstract Viewer/Itinerary Planner [Internet]. Washington (DC): Society for Neuroscience.

Hallermann S, Pawlu C, Jonas P, Heckmann M. 2003. A large pool of releasable vesicles in a cortical glutamatergic synapse. Proc Natl Acad Sci USA. 100:8975–8980.

Harris KM, Sultan P. 1995. Variation in the number, location and size of synaptic vesicles provides an anatomical basis for the nonuniform probability of release at hippocampal CA1 synapses. Neuropharmacology. 34:1387–1395.

Hilfiker S, Pieribone VA, Czernik AJ, Kao HT, Augustine GJ, Greengard P. 1999. Synapsins as regulators of neurotransmitter release. Philos Trans R Soc Lond B Biol Sci. 354:269–279.

Hilfiker S, Schweizer FE, Kao HT, Czernik AJ, Greengard P, Augustine GJ. 1998. Two sites of action for synapsin domain E in regulating neurotransmitter release. Nat Neurosci. 1:29–35.

Hjorth-Simonsen A. 1973. Some intrinsic connections of the hippocampus in the rat: an experimental analysis. J Comp Neurol. 147:145–161.

Hvalby O, Jensen V, Kao HT, Walaas SI. 2006. Synapsin-regulated synaptic transmission from readily releasable synaptic vesicles in excitatory hippocampal synapses in mice. J Physiol. 571:75–82.

Jensen V, Walaas SI, Hilfiker S, Ruiz A, Hvalby OC. 2007. A delayed response enhancement during hippocampal presynaptic plasticity in mice. J Physiol. 583:129–143.

Kao HT, Li P, Chao HM, Janoschka S, Pham K, Feng J, Mcewen BS, Greengard P, Pieribone VA, Porton B. 2008. Early involvement of synapsin III in neural progenitor cell development in the adult hippocampus. J Comp Neurol. 507(6):1860–1870.

Kao HT, Porton B, Czernik AJ, Feng J, Yiu G, Haring M, Benfenati F, Greengard P. 1998. A third member of the synapsin gene family. Proc Natl Acad Sci USA. 95:4667–4672.

Kielland A, Erisir A, Walaas SI, Heggelund P. 2006. Synapsin utilization differs among functional classes of synapses on thalamocortical cells. J Neurosci. 26:5786–5793.

Kim CH, Lisman JE. 1999. A role of actin filament in synaptic transmission and long-term potentiation. J Neurosci. 19:4314–4324.

Lisman JE, Raghavachari S, Tsien RW. 2007. The sequence of events that underlie quantal transmission at central glutamatergic synapses. Nat Rev Neurosci. 8:597–609.

McMahon HT, Nicholls DG. 1991. Transmitter glutamate release from isolated nerve terminals: evidence for biphasic release and triggering by localized Ca^{2+}. J Neurochem. 56:86–94.

Millar AG, Bradacs H, Charlton MP, Atwood HL. 2002. Inverse relationship between release probability and readily releasable vesicles in depressing and facilitating synapses. J Neurosci. 22:9661–9667.

Mori M, Abegg MH, Gahwiler BH, Gerber U. 2004. A frequency-dependent switch from inhibition to excitation in a hippocampal unitary circuit. Nature. 431:453–456.

Nicoll RA, Schmitz D. 2005. Synaptic plasticity at hippocampal mossy fibre synapses. Nat Rev Neurosci. 6:863–876.

Pieribone VA, Porton B, Rendon B, Feng J, Greengard P, Kao HT. 2002. Expression of synapsin III in nerve terminals and neurogenic regions of the adult brain. J Comp Neurol. 454:105–114.

Pieribone VA, Shupliakov O, Brodin L, Hilfiker-Rothenfluh S, Czernik AJ, Greengard P. 1995. Distinct pools of synaptic vesicles in neurotransmitter release. Nature. 375:493–497.

Rollenhagen A, Sätzler K, Rodríguez EP, Jonas P, Frotscher M, Lübke JH. 2007. Structural determinants of transmission at large hippocampal mossy fiber synapses. J Neurosci. 27:10434–10444.

Rosahl TW, Spillane D, Missler M, Herz J, Selig DK, Wolff JR, Hammer RE, Malenka RC, Sudhof TC. 1995. Essential functions of synapsins I and II in synaptic vesicle regulation. Nature. 375:488–493.

Ryan TA, Li L, Chin LS, Greengard P, Smith SJ. 1996. Synaptic vesicle recycling in synapsin I knock-out mice. J Cell Biol. 134:1219–1227.

Ryan TA, Reuter H. 2001. Measurements of vesicle recycling in central neurons. News Physiol Sci. 16:10–14.

Sakaba T, Neher E. 2003. Involvement of actin polymerization in vesicle recruitment at the calyx of Held synapse. J Neurosci. 23:837–846.

Salin PA, Scanziani M, Malenka RC, Nicoll RA. 1996. Distinct short-term plasticity at two excitatory synapses in the hippocampus. Proc Natl Acad Sci USA. 93:13304–13309.

Sankaranarayanan S, Atluri PP, Ryan TA. 2003. Actin has a molecular scaffolding, not propulsive, role in presynaptic function. Nat Neurosci. 6:127–135.

Schikorski T, Stevens CF. 1997. Quantitative ultrastructural analysis of hippocampal excitatory synapses. J Neurosci. 17:5858–5867.

Shupliakov O, Bloom O, Gustafsson JS, Kjaerulff O, Low P, Tomilin N, Pieribone VA, Greengard P, Brodin L. 2002. Impaired recycling of synaptic vesicles after acute perturbation of the presynaptic actin cytoskeleton. Proc Natl Acad Sci USA. 99:14476–14481.

Siksou L, Rostaing P, Lechaire JP, Boudier T, Ohtsuka T, Fejtova A, Kao HT, Greengard P, Gundelfinger ED, Triller A, et al. 2007. Three-dimensional architecture of presynaptic terminal cytomatrix. J Neurosci. 27:6868–6877.

Spillane DM, Rosahl TW, Sudhof TC, Malenka RC. 1995. Long-term potentiation in mice lacking synapsins. Neuropharmacology. 34:1573–1579.

Stevens CF, Wesseling JF. 1998. Activity-dependent modulation of the rate at which synaptic vesicles become available to undergo exocytosis. Neuron. 21:415–424.
Takei Y, Harada A, Takeda S, Kobayashi K, Terada S, Noda T, Takahashi T, Hirokawa N. 1995. Synapsin I deficiency results in the structural change in the presynaptic terminals in the murine nervous system. J Cell Biol. 131:1789–1800.
Tao-Cheng JH. 2006. Activity-related redistribution of presynaptic proteins at the active zone. Neuroscience. 141:1217–1224.
Tao-Cheng JH, Dosemeci A, Winters CA, Reese TS. 2006. Changes in the distribution of calcium calmodulin-dependent protein kinase II at the presynaptic bouton after depolarization. Brain Cell Biol. 35:117–124.
Terada S, Tsujimoto T, Takei Y, Takahashi T, Hirokawa N. 1999. Impairment of inhibitory synaptic transmission in mice lacking synapsin I. J Cell Biol. 145:1039–1048.
Wickelgren WO, Leonard JP, Grimes MJ, Clark RD. 1985. Ultrastructural correlates of transmitter release in presynaptic areas of lamprey reticulospinal axons. J Neurosci. 5:1188–1201.
Witter MP, Naber PA, van Haeften T, Machielsen WC, Rombouts SA, Barkhof F, Scheltens P, Lopes da Silva FH. 2000. Cortico-hippocampal communication by way of parallel parahippocampal-subicular pathways. Hippocampus. 10:398–410.
Zucker RS, Regehr WG. 2002. Short-term synaptic plasticity. Annu Rev Physiol. 64:355–405.